Molecular Microbiology (2008) 70(6), 1397–1407 ■
doi:10.1111/j.1365-2958.2008.06486.x
First published online 24 October 2008

Clustering and dynamics of cytochrome *bd*-I complexes in the *Escherichia coli* plasma membrane *in vivo*

Tchern Lenn,[1†] Mark C. Leake[2,3†] and Conrad W. Mullineaux[1*]
[1]*School of Biological and Chemical Sciences, Queen Mary, University of London, Mile End Road, London E1 4NS, UK.*
[2]*Clarendon Laboratory, Department of Physics, University of Oxford, Parks Road, Oxford OX1 3PU, UK.*
[3]*Oxford Centre for Integrative Systems Biology (OCISB), Department of Biochemistry, University of Oxford, South Parks Road, Oxford OX1 3QU, UK.*

Summary

The cytochrome *bd*-I complex of *Escherichia coli* is a respiratory terminal oxidase and an integral component of the cytoplasmic membrane. As with other respiratory components, the organization and dynamics of this complex in living membranes is unknown. We set out to visualize the distribution and dynamics of this complex *in vivo*. By exchanging *cydB* for *cydB–gfpgcn4* on the *E. coli* chromosome, we produced a strain (YTL01) that expresses functional GFP-tagged cytochrome *bd*-I terminal oxidase complexes under wild-type genetic control. We imaged live YTL01 cells using video-rate epifluorescence and total internal reflection fluorescence (TIRF) microscopy in combination with fluorescence recovery after photobleaching (FRAP) and saw mobile spots of GFP fluorescence in plasma membranes. Numbers of GFP molecules per spot were quantified by step-wise photobleaching giving a broad distribution with a mean of ~76, indicating that cytochrome *bd*-I is concentrated in mobile patches in the *E. coli* plasma membrane. We hypothesize that respiration occurs in mobile membrane patches which we call 'respirazones'.

Introduction

Oxidative phosphorylation (OXPHOS) is a multistep membrane process, which is the result of the concerted activities of multiple enzymes. These enzymes have been best characterized in mammalian mitochondria, where they are found in the inner mitochondrial membrane. In prokaryotes, the OXPHOS membrane is usually the plasma membrane. Research on this subject continues to focus mainly on the structure and function of the individual OXPHOS complexes (for review see Rich, 2003) and regulation of expression at the transcriptional level in prokaryotes (for review see Unden and Bongaerts, 1997). Relatively little is known about the supramolecular organization and interactions of OXPHOS complexes in intact bioenergetic membranes. Two contrasting models of organization have been proposed. For a review of the debate, see Lenaz and Genova (2007). The Random Diffusion model proposes that there is no large-scale organization of complexes: they are randomly dispersed and functionally connected mainly by lateral diffusion of small redox carriers. 'Solid-state' models however suggest that electron transport happens within stable supercomplexes of the respiratory proteins. In agreement with this idea, OXPHOS supercomplexes or 'respirasomes' have been isolated from membranes of mammalian, plant and yeast mitochondria and the bacterium *Paracoccus denitrificans* by blue-native polyacrylamide gel electrophoresis (BN-PAGE) (Schägger, 2002). Structures of these supercomplexes have been resolved by single-particle cryo-electron microscopy (Dudkina *et al.*, 2006; Schäfer *et al.*, 2006).

More generally, the traditional Fluid Mosaic Model of biological membranes (Singer and Nicholson, 1972) is being supplanted by the 'Partitioned' or 'Compartmentalized Fluid' model (Engelman, 2005; Kusumi *et al.*, 2005; Marguet *et al.*, 2006). This new membrane paradigm sees non-random distributions of membrane proteins as the norm rather than the exception.

An attractive approach to studying the organization and dynamics of membrane proteins *in vivo* is to use gene fusions to tag proteins with green fluorescent protein (GFP) or variants. Fluorescence microscopy can then be used to observe the behaviour of the protein in the intact membrane. Such an approach has been applied to OXPHOS complexes by Johnson *et al.* (2004). These authors showed that OXPHOS complexes (ATP synthase and succinate dehydrogenase) are heterogeneously distributed in mobile patches in the *Bacillus subtilis* plasma membrane. However, the genes

Accepted 30 September, 2008. *For correspondence. E-mail c.mullineaux@qmul.ac.uk; Tel. (+44) 20 7882 7008; Fax (+44) 20 8983 0973. †These authors contributed equally to the work.

were expressed using heterologous promoters, raising the possibility of artefacts due to overexpression and expression of complexes in a non-physiological context. The dynamic localization of the proteins was investigated only at low time resolution (frames recorded at 1 min intervals) and the number of GFP molecules in the mobile patches was not quantified.

We set out to investigate the question further by GFP tagging of OXPHOS complexes in the plasma membrane of *Escherichia coli*. In contrast to mammalian and plant mitochondria, *E. coli* possess multiple, branched electron transport chains that are employed under various conditions to perform OXPHOS, depending on substrate availability (Unden and Bongaerts, 1997). In our study we investigate the cytochrome *bd*-I complex, which is encoded by the *cyd*AB operon. In aerobic respiration, the cytochrome *bd*-I complex is one of two terminal oxidases that catalyse the final transfer of electrons from ubiquinol to molecular oxygen. The complex has been characterized as a heterodimer: subunit 1, encoded by *cyd*A, is a 57 kDa haem-binding protein and a *b*-type cytochrome; subunit 2, encoded by *cydB*, is a 43 kDa haem-binding protein and a *d*-type cytochrome (Miller and Gennis, 1983). It is maximally expressed in cells under microaerobic conditions, but is relatively repressed under aerobic and anaerobic conditions. Transcription of the other ubiquinol oxidoreductase, the 4-subunit cytochrome *bo* complex, encoded by the *cyoABCD* operon, is however, contrastingly induced in aerobic conditions and repressed in microaerobic and anaerobic conditions (Cotter *et al*., 1990; Iuchi *et al*., 1990). The two complexes are spectroscopically distinct. Another *bd*-type complex encoded by the *cyx* or *cbd* operon exists in the *E. coli* genome but it does not appear to have respiratory function in wild-type cells (Dassa *et al*., 1991; Sturr *et al*., 1996).

Here we have applied live-cell fluorescence imaging techniques to document the organization and dynamics of functional GFP-tagged cytochrome *bd*-I complexes in living *E. coli* cells on a millisecond timescale. We engineered an *E. coli* strain, YTL01, which expresses functional GFP-tagged cytochrome *bd*-I complexes from the native chromosomal locus and is therefore under wild-type genetic control. In YTL01 cells, we see fast-moving patches of GFP fluorescence in the plasma membrane, indicating that the cytochrome *bd*-I complex is localized into mobile membrane domains. Furthermore we are able to track the motion of individual patches and deduce the number of GFP molecules, and hence cytochrome *bd* complexes, present in them, from bleaching kinetics. We suggest that in *E. coli*, patches of the plasma membrane are dedicated to respiratory function by the preference of respiratory complexes to localize within these domains.

Results

Construction of E. coli *strain YTL01, expressing CydB–GFP*

The C-terminus of the CydB subunit of the cytochrome *bd*-I complex is exposed on the cytoplasmic side of the membrane and appears not to be close to the active site of the complex (Zhang *et al*., 2004). Thus it is a promising location for addition of a GFP tag. We used as a starting point a *cydB–gfp* fusion construct available from the ASKA Library (Kitagawa *et al*., 2005). This construct codes for CydB with an N-terminal His-tag and C-terminus tagged with a GFPuv4 (Ito *et al*., 1999) linked to CydB by a five-amino-acid spacer. The *cydB–gfpgcn4* gene (without the His-tag) was transferred into the chromosomal *cydB* locus of *E. coli* BW25113 via a suicide vector as detailed in *Experimental procedures* and illustrated in Fig. 1. Candidate colonies were screened by fluorescence microscopy and colony PCR with primers that flanked the recombination sites. We found one colony with green fluorescence and this was also the only colony to give a PCR product of the expected size. Sequencing of the PCR product showed no mutations in the *cydB* domain (although there is a point mutation in the GFP tag: a C:T substitution at base 231 of the *gfpgcn4* domain converts a histidine residue to tyrosine). Thus, as illustrated in Fig. 1, we produced a strain that is genetically identical to BW25113 with the exception of the substitution of *cydB–gfpgcn4* for the wild-type *cydB*.

Characterization of CydB–GFP expression and function

Figure 2 shows a series of tests for the expression and functionality of CydB–GFP *in vivo.* YTL01 cultures were grown overnight in aerobic batch culture in LB medium and cells were fractionated into membrane, cytoplasmic

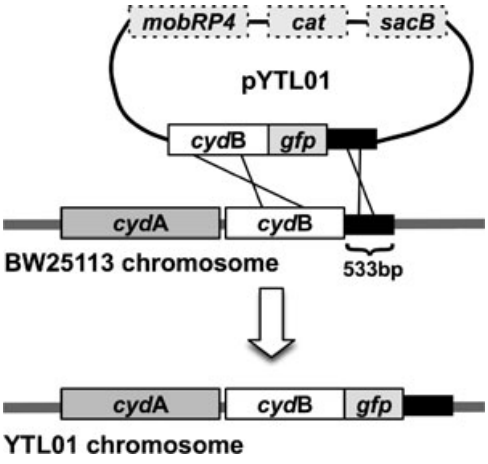

Fig. 1. Construction of *Escherichia coli* YTL01: insertion of GFP into the BW25113 chromosome downstream of the *cydB* locus.

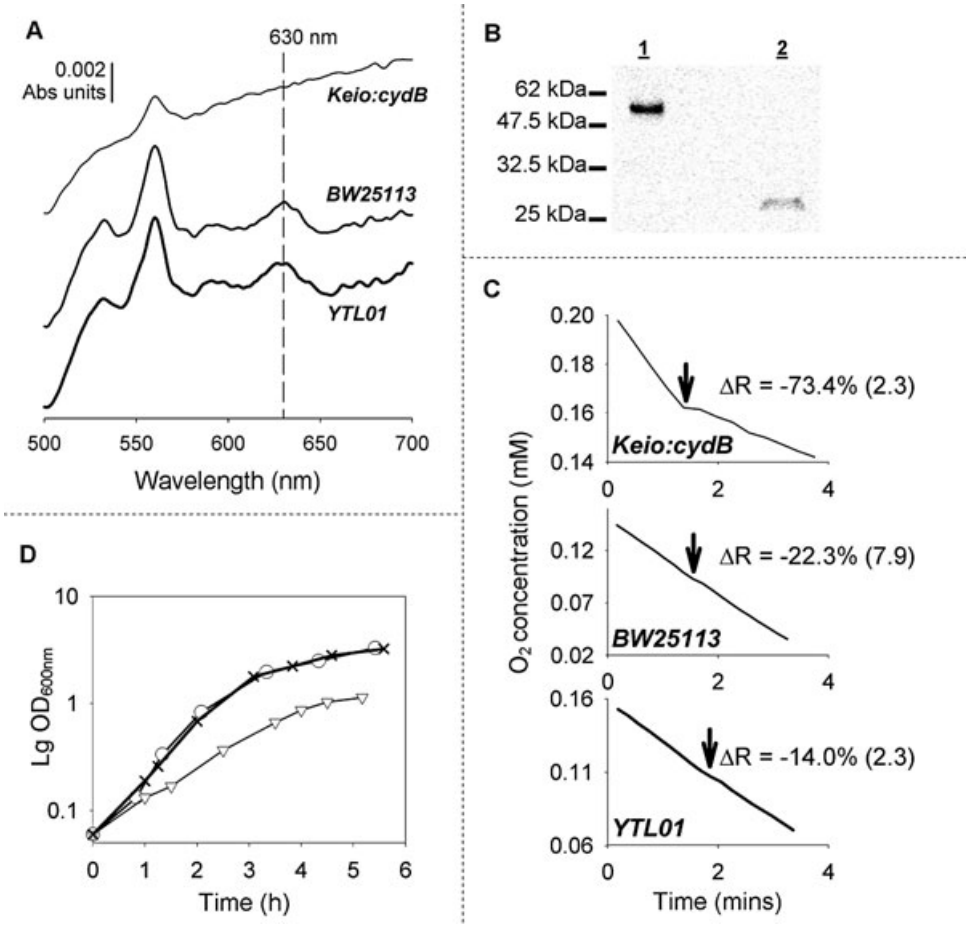

Fig. 2. Characterization of *E. coli* YTL01.
A. Reduced-minus-oxidized difference spectra of YTL01 cells in early stationary phase.
B. Immunoblot with anti-GFP antibodies: lane 1, YTL01 membrane fraction; lane 2, GFP standard.
C. Oxygen electrode traces showing the effect of 30 mM hydroxylamine on respiration of *E. coli* cultures. Arrows indicate the addition of hydroxylamine to a final concentration of 30 mM. ΔR values are the mean percentage change in respiratory rate upon addition of hydroxylamine of five replicate experiments, with standard deviation given in parentheses.
D. Representative growth of *E. coli* batch cultures: BW25113 (○), YTL01 (×) and Keio:*cydB* (▽).

and periplasmic fractions. Western blots of cell fractions with an anti-GFP antibody show a single band in the membrane fraction at ~50 kDa compared with free GFP at ~28 kDa (Fig. 2B). The observed band is very close to the 56 kDa band predicted for the GFP-tagged CydB complex since CydB runs as a 28 kDa band in 12.5% acrylamide SDS-PAGE (Kita *et al*., 1984). No GFP was detected in any of the other YTL01 fractions or any BW25113 fractions (data not shown). Thus there is no indication of any free GFP in the cells: any GFP fluorescence detected from the cells indicates the position of cytochrome *bd*-I complexes.

Fluorescence microscopy (detailed below) confirms that GFP fluorescence is associated with the plasma membrane. We saw no evidence of GFP association with inclusion bodies or other artefactual aggregates. In preliminary experiments in which we overexpressed CydB–GFP from a plasmid we observed large, bright, immobile patches of GFP fluorescence (not shown). However, we could not detect any such bodies in YTL01 cells.

Levels of cytochrome *bd*-I were quantified by room temperature absorption difference spectra (dithionite reduced-minus-air oxidized) (Green and Gennis, 1983). For these measurements we used cells grown to late exponential/early stationary phase in aerobic batch culture in LB medium. We found that growth to late exponential phase was necessary to give an absorption difference large enough to be quantifiable. However, even under these conditions, which appear to promote the highest levels of cytochrome *bd*-I expression, the difference spectrum is a small signal on a large background of cell absorption and scattering, and therefore we cannot measure cytochrome *bd*-I levels accurately. YTL01 and wild-type cells show a broad absorption peak centred at

~630 nm, consistent with the haem *d* in subunit 2 of the complex, encoded by *cydB* (Green and Gennis, 1983). This peak is absent in the *cydB*-null mutant from the Keio Collection (Baba *et al*., 2006) (Fig. 2A). These spectra show that cytochrome *bd*-I is present in YTL01 cells at approximately wild-type levels. Using the extinction coefficient of 27.9 mM^{-1} cm^{-1} for the 628–651 nm wavelength pair (Tsubaki *et al*., 1995), we can estimate that there are approximately 30 000–40 000 cytochrome *bd*-I complexes per cell in wild-type and YTL01 cells under these conditions.

To determine whether the GFP-tagged cytochrome *bd*-I complexes in YTL01 are functional for electron transport, we examined the effect of the respiratory inhibitor hydroxylamine on aerobic respiration in YTL01, wild-type and *cydB*-null cells from mid-exponential-phase aerobic batch cultures (Fig. 2C). Hydroxylamine has a much larger inhibitory effect on the cytochrome *bo* oxidase than *bd* (Meunier *et al*., 1995). Oxygen consumption by cells in the presence of hydroxylamine therefore indicates cytochrome *bd*-I activity as cytochrome *bo* is inhibited. As expected, respiration in *cydB*-null cells is sensitive to 30 mM hydroxylamine. In contrast, YTL01 cells, like wild-type cells, are relatively insensitive to hydroxylamine (Fig. 2C). This shows that the GFP tag on CydB does not interfere with the electron transport activity of the complex. Furthermore, the growth of YTL01 and wild-type strains in batch culture are similar whereas *cydB*-null cells grow much more slowly (Fig. 2D). Our results show that CydB–GFP is as active as the wild-type protein.

Visualization of GFP fluorescence

GFP fluorescence in YTL01 cells was visualized using both epifluorescence and total internal reflection fluorescence (TIRF) microscopy. TIRF microscopy is essentially a modification of epifluorescence microscopy in which the laser excitation beam is directed at a very shallow angle so that it reflects off the interface between a glass coverslip and the aqueous medium containing the biological sample. Under these conditions an evanescent wave penetrates beyond the interface into the sample. The light intensity decays exponentially with distance from the interface, providing a working depth of field which is a function of the wavelength of the laser, and is about 100 nm for our experiments here. Therefore TIRF microscopy effectively gives an optical section of approximately 100 nm in thickness at the coverslip–sample interface and is ideal for visualizing fluorophores in bacterial cell membranes, with minimal background from autofluorescence from the cytoplasm (Leake *et al*., 2006). We used video-rate (25 Hz) image acquisition. Individual frames show the instantaneous distribution of fluorescence within the cell, whereas frame averages show the mean distribution over time.

Cells for fluorescence microscopy were grown overnight to stationary phase, then diluted 10-fold in fresh, oxygenated minimal medium a few hours prior to the measurements. The use of minimal medium was necessary to avoid background fluorescence from the LB broth. During fluorescence microscopy the cells were immobilized by adhesion to a polylysine-coated glass coverslip, and trapped in 5–10 μl of medium between the coverslip and a microscope slide. Two sides of the flow cell were left open to the air; however, the arrangement did not allow us to control oxygen levels in the medium during the 1–2 h time span of the fluorescence measurements. Oxygen concentration would have decreased during this time if respiration by the cells were faster than replenishment of oxygen from the atmosphere at the edges of the coverslip. Since cytochrome *bd*-I expression is influenced by the oxygenation of the medium (Cotter *et al*., 1990) we checked to see if mean cellular GFP fluorescence changed over the time span of the measurements. However, we could see no significant trend (data not shown).

Frame-averaged images obtained using epifluorescence with the focal plane set at mid-cell height show a halo-like appearance around the perimeter of the cell, indicative of membrane localization (Fig. 3A). Frame-averaged TIRF images show localization in the membrane segment within ~100 nm of the coverslip surface (Fig. 3B). Observations of single cells in individual image frames at 25 Hz time resolution indicate the presence of fluorescent spots of apparent diameter ~400 nm diffusing in the cell membrane (Fig. 3C). Figure 3C shows a frame with a particularly clear set of bright, distinct fluorescent spots. For a more complete impression of the distribution and dynamics of fluorescence see Movie S1. The spots show heterogeneous fluorescence intensity and diffuse in the membrane over a timescale of tens of milliseconds (Fig. 3C, Movie S1). The heterogeneity in spot brightness indicates that spots consist of clusters containing variable numbers of GFP-tagged cytochrome *bd*-I complexes. Individual spots could sometimes be tracked for over a second before they left the field of view. On this timescale we could see no direct indication of additional dimmer spots breaking away or coalescing with a given tracked spot. This suggests that there is minimal dissociation or re-association of GFP-tagged complexes within this time window.

To permit detailed analysis on individual fluorescent spots, we improved the imaging contrast further by rapidly photobleaching one of the poles of each cell under investigation using an intense focused laser of width ~1 μm (Fig. 3D). This allowed us to monitor fluorescencerecovery after photobleaching (FRAP) on a video-

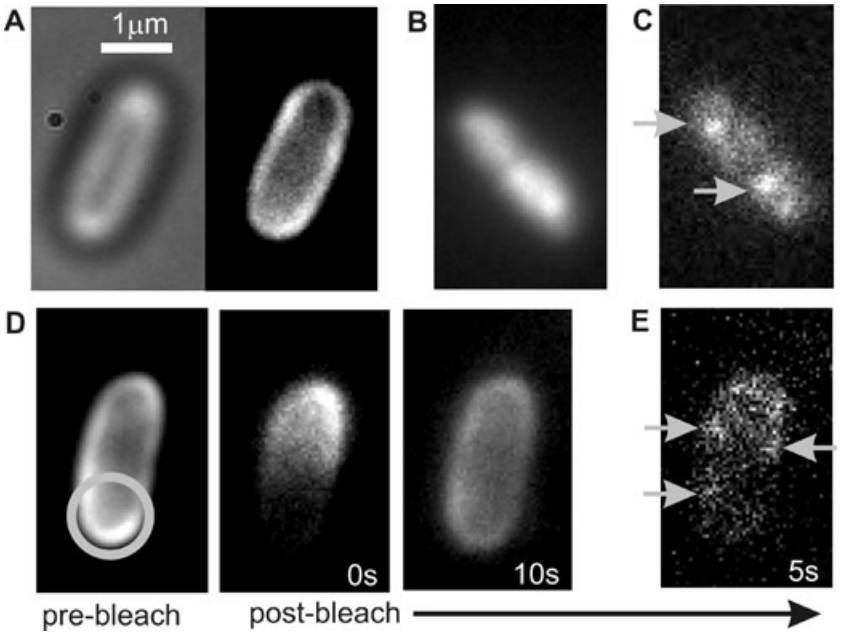

Fig. 3. Visualization of GFP fluorescence in *E. coli* YTL01.
A. Bright-field (left) and epifluorescence images (right, frame-averaged over 2 s) of the same cell, focal plane 500 nm from coverslip surface.
B and C. (B) TIRF images of a cell (frame-averaged over 2 s) and (C) individual 40 ms frame [autodetected fluorescent spots indicated (arrows), focal plane 100 nm from coverslip surface].
D. Epifluorescence images before and after bleaching one end of the cell. The circle indicates the laser focus width. Images 0 s and 10 s after bleaching are frame-averaged over 2 s.
E. The same cell 5 s after FRAP bleach showing individual 40 ms frame with autodetected fluorescent spots (arrows).

rate timescale fast enough to track individual diffusing spots in either TIRF mode (Movie S2) or epifluorescence mode (Fig. 3E, Movie S3).

Quantitative analysis of fluorescence images

Using robust custom-written tracking software utilizing both automated detection and iterative Gaussian masking of pixel intensities (Leake *et al*., 2006; 2008) the positions of spots could be calculated to within a few nanometres precision (see Supporting Method S2 for details). In addition, using a method based on the step-wise photobleaching of individual GFP fluorophores (Leake *et al*., 2006) we could estimate the number of CydB–GFP molecules in each spot (see Supporting Method S3 for details). The distribution is broad and roughly Gaussian with a mean of 76 ± 33 CydB–GFP molecules per spot (Fig. 4). Fourier frequency analysis of the distribution indicates a characteristic spacing of ~4 CydB–GFP molecules (Fig. 4, inset). This may indicate that the fundamental structural unit of cytochrome *bd*-I within a cluster is a tetramer. We estimate that there are on average 230 ± 80 clusters per cell. The calculation is detailed in Supporting Method S2: it depends on extrapolation from the limited region of the cell membrane that we observe in epifluorescence measurements. Note that in both epifluorescence images (Fig. 3C) and TIRF images (Fig. 3D) only a fraction of the membrane surface is within the field of view. We estimate about 10% in both cases. We can estimate that about 17 500 ± 9900 CydB–GFP molecules per cell are associated directly with the clusters, and 2300 ± 830 CydB–GFP per cell are present in the membrane but not confined in clusters (calculation detailed in Supporting Method S3). This leads to an estimated total of roughly 19 800 ± 9900 CydB–GFP molecules per cell. We estimate 30 000–40 000 cytochrome *bd* per cell from absorption difference spectra (Fig. 2A). Since this is a little higher than the mean number of GFP molecules per cell it suggests that at least the vast majority of CydB–GFP are fully assembled and redox-active. There is some uncertainty in both estimates of cellular CydB content, but the slight discrepancy in the numbers could also be due to the slightly different treatment of the cells (see *Experimental procedures*, and discussion above). However, we could not detect any significant change in mean GFP

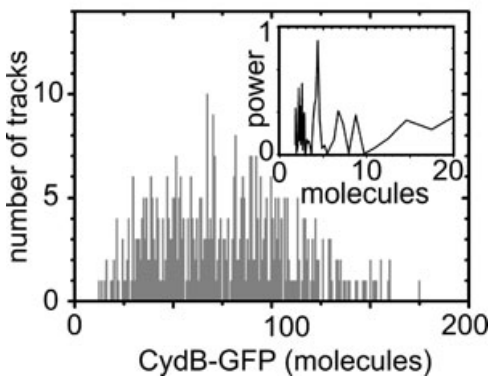

Fig. 4. Stoichiometry of CydB–GFP complexes. Distribution estimated using step-wise photobleaching (Leake *et al*., 2006; 2008) of GFP of tracked fluorescent spots. The power spectrum of the distribution (inset) indicates a periodicity of ~4 CydB–GFP molecules per complex.

fluorescence intensity as a function of time during the course of the fluorescence microscopy.

Our main data sets were recorded for cells at room temperature (about 20°C). However, we also observed a qualitatively similar distribution of GFP fluorescence in cells at 37°C (not shown). In general, the formation of the CydB–GFP clusters appears very robust. We saw no significant trends in mean GFP per cluster, or mean number of clusters per cell, as a function of time on the coverslip during the 1–2 h time-course of the fluorescence measurements (not shown). We saw considerable variation among cells in total GFP fluorescence, indicating widely varying levels of cytochrome *bd*-I expression in individual cells. There was a trend towards increasing GFP per cluster in cells with higher total GFP fluorescence (not shown). However, all cells showed qualitatively the same pattern of clustering of GFP fluorescence. Thus the formation of the cytochrome *bd*-I clusters does not appear particularly sensitive to the concentration of cytochrome *bd*-I in the membrane.

To analyse diffusion of spots in the cell membrane we transformed the spot position co-ordinates which were recorded in the Cartesian plane of the camera detector into a curvilinear system to represent the unique cell surface based on the length, width and orientation of each individual cell as measured from the non-fluorescence bright-field image (Leake *et al.*, 2008). We then constructed a mean-squared displacement function (*MSD*) for each track, defined as follows (Gross and Webb, 1988):

$$MSD(\tau) = MSD(n\Delta t) = \frac{1}{N-1-n}\sum_{i=1}^{N-1-n}\{[x'(i\Delta t + n\Delta t) - x'(i\Delta t)]^2 + [y'(i\Delta t + n\Delta t) - y'(i\Delta t)]^2\}$$

A track consists of N consecutive image frames with a time interval τ ($n\Delta t$). Averaging all tracks showed deviation from linearity indicating anomalous diffusion behaviour (Fig. 5A). However, tracks could be separated on the basis of diffusive mode into either normal Brownian diffusion or restricted diffusion, using the relative deviation parameter which is defined as unity for pure Brownian diffusion and lower values for restricted diffusion (Kusumi *et al.*, 1993). See Supporting Method S4 for further details. The mean normal diffusion *MSD* function was fitted well by a straight line, indicating a diffusion coefficient of 0.05 ± 0.02 $\mu m^2\ s^{-1}$ (Fig. 5B). The mean restricted diffusion *MSD* function was fitted using a mobility-confinement model (Kusumi *et al.*, 1993), indicating that the effective diameter of the confining zone is 160 ± 30 nm (Fig. 5C). Binning individual normal diffusion tracks on the basis of estimated CydB–GFP stoichiometry indicated an approximately inverse relationship between the stoichiometry and measured diffusion coefficient (Fig. 5D).

Figure 6A (black histogram) shows the apparent diameter of the fluorescent spots (defined as twice the fitted $1/e^2$ Gaussian radius) measured using TIRF illumination to avoid defocusing artefacts from epifluorescence. There is a broad spread, with a mean of 370 ± 80 nm. However, the real dimensions of the membrane patches must be considerably smaller than this, since the blurring due to limited optical resolution is very significant at these scales. When fluorescence from a single GFP molecule is imaged in our microscope, it appears as a spot with mean diameter 270 ± 30 nm (Fig. 6A, grey histogram) which approximates to the point-spread function of the microscope. The difference between the two diameters gives a rough estimate of the real physical dimensions of

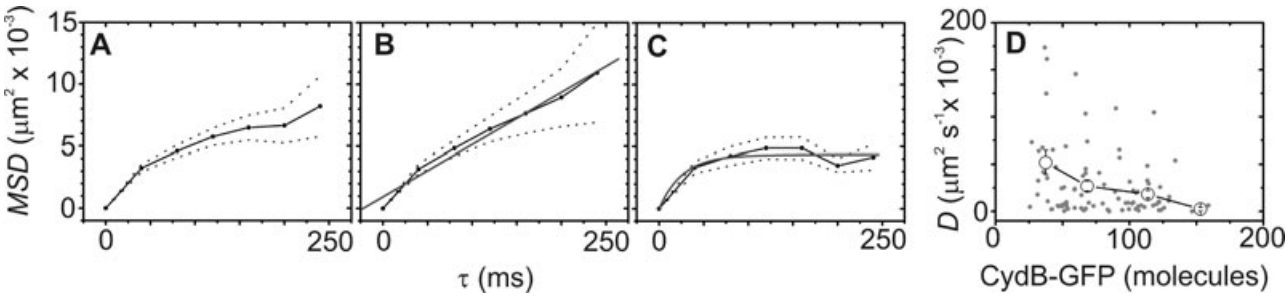

Fig. 5. Mobility of tracked CydB–GFP complexes.
A. Estimate of mean-squared displacement (*MSD*) assuming two-dimensional diffusion over the cell membrane surface (mean of 103 tracks, standard deviation error bounds indicated).
B. *MSD* (black, dotted error bounds) for normal diffusion tracks such that relative deviation parameter > 0.3, showing mean of 61 tracks with linear fit.
C. *MSD* (black, dotted error bounds) for confined diffusion tracks such that relative deviation parameter ≤ 0.3, showing mean of 43 tracks with restricted diffusion fit (Kusumi *et al.*, 1993) for which asymptotic values of *MSD* approach $L^2/6$ where L is the effective diameter of a confinement zone.
D. Variation of estimated *MSD* with stoichiometry (grey), with binned values indicated (black).

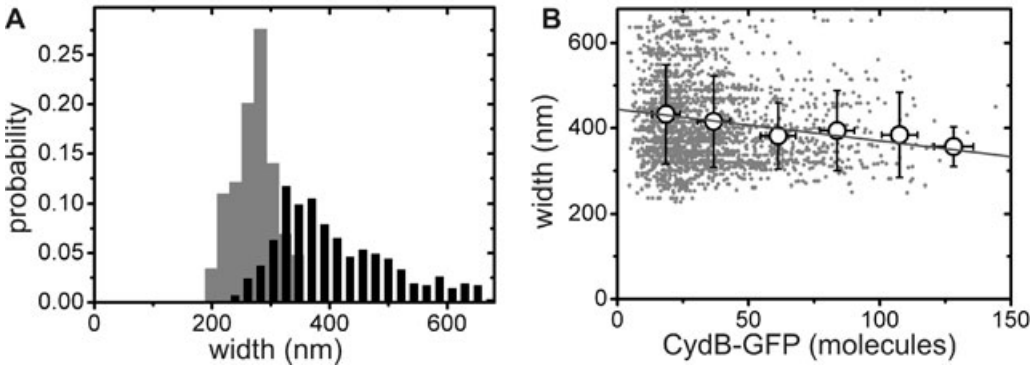

Fig. 6. A. Variation in fluorescent spot diameter using TIRF illumination on purified, surface-immobilized GFP (Leake *et al*., 2006) indicated in grey, compared against fluorescent spots observed *in vivo* in YTL01 cells (black).
B. Variation of spot width with estimated number of CydB–GFP molecules per complex (grey, binned value black with standard deviation error bars) with linear fit.

the clusters (since fluorophores at the edge of the patch will produce fluorescence blurred out to a radius of about 135 nm beyond the boundary of the patch). Thus we can estimate a mean patch diameter of about 100 nm. Surprisingly, the variation in apparent spot diameter was independent of the number of GFPs per spot (Fig. 6B), thus the number of cytochrome *bd*-I complexes per spot is not directly related to the area of the membrane patch.

Discussion

Our results show that the cytochrome *bd*-I terminal oxidase in *E. coli* is concentrated in mobile domains in the membrane. This is qualitatively similar to the report of Johnson *et al*. (2004) on the dynamic localization of succinate dehydrogenase and ATP synthase in *B. subtilis*. However, our methodology yields a level of quantitative detail on organization and dynamics that is unprecedented for any respiratory protein. The GFP-fusion protein is expressed from its native locus, meaning that transcriptional regulation of the construct is under wild-type control. This eliminates the possibility that our observations are artefacts due to overexpression and/or expression in a non-physiological context. Furthermore, we find no significant physiological differences between wild-type and YTL01 cells. This strongly suggests that the observed distribution of cytochrome *bd*-I complexes is physiologically relevant, since we would expect abnormal distribution of the complex to result in abnormal function.

The live-cell imaging apparatus used is sensitive enough to distinguish the fluorescence signal of single GFP molecules from background electronic noise without frame averaging or long exposure times (Leake *et al*., 2006). This sensitivity is mainly conferred by the electron-multiplying charge-coupled device (EMCCD) camera technology used but is further enhanced by using the apparatus in TIRF mode, where selective excitation of fluorophores close to the coverslip removes 'pollution' of the signal from out-of-focus fluorescence and cytoplasmic autofluorescence. In addition, FRAP-style pre-bleaching removes considerable background fluorescence and results in a significantly improved imaging contrast. The high sensitivity of the apparatus allows for images with meaningful signal-to-noise ratios to be captured at video rate, allowing us to observe events that happen on a short (tens of milliseconds) timescale and resolve mobile structures without blurring. Using these high-speed imaging techniques in combination with single-particle tracking analysis, we have not only been able to observe clustering of the cytochrome *bd*-I complex, but also we could (i) quantitatively estimate the number of complexes within a cluster to a precision of single molecules, (ii) obtain a distribution of cluster sizes within a single cell, (iii) accurately characterize the mobility of the observed clusters with spatial resolution of a few nanometres, and (iv) estimate the real diameter of the clusters.

The mobile assemblages of the cytochrome *bd*-I complex are on a much larger scale than respiratory supercomplexes identified by biochemical means. The largest biochemically characterized supercomplexes contain only four to six electron transport complexes (Boekema and Braun, 2007). In contrast, the assemblages that we observe *in vivo* contain on average about 76 cytochrome *bd*-I complexes. The assemblages are too small for us to be able to measure their physical dimensions accurately, but we can estimate a mean diameter of ~100 nm. This would correspond to a membrane area of ~8000 nm^2. Since no structure is available for cytochrome *bd*-I we cannot be sure of the membrane area occupied by a single complex. However, we can estimate this based on the predicted 17 transmembrane alpha helices of the cytochrome *bd* complex (Zhang *et al*., 2004). By extrapolation from the transmembrane portion of fumarate reductase, which has six membrane-spanning alpha

helices and a diameter of ~3.8 nm (Iverson *et al*., 1999), we can estimate an area of ~32 nm^2. So 76 cytochrome *bd*-I complexes would occupy a membrane area of ~2400 nm^2, only about 30% of the mean area of the membrane patches. Furthermore, apparent spot width does not increase with the number of cytochrome *bd*-I complexes (Fig. 6B), and there is a broad distribution of apparent widths of spots with the same number of CydB–GFP molecules. This suggests that the fluorescent spots observed mark patches of membrane containing rather loose assemblages of cytochrome *bd*-I complexes, as opposed to cytochrome *bd*-I multimers held together by strong, stable dimer–dimer interactions. By our estimates, these patches are large enough to contain other proteins as well. Preliminary results from GFP tagging suggest that other *E. coli* OXPHOS complexes including NDH-2 (T. Lenn, M.C. Leake and C.W. Mullineaux, unpublished) and Complex I, Complex II and Complex V (T. Friedrich, pers. comm.) are also heterogeneously distributed in the membrane. We cannot yet be sure whether these OXPHOS complexes are all located in the same respiratory patches, or whether each complex is concentrated in separate patches. Careful colocalization studies will be needed to answer the question. However, we can estimate that, in an average cell, the cytochrome *bd*-I patches will occupy about 23% of the membrane area. It seems unlikely that there could be space in the membrane for similar, separate patches of the other OXPHOS complexes, plus the numerous other protein structures that must be accommodated in the membrane. This suggests that colocalization of other OXPHOS complexes within the cytochrome *bd*-I patches is likely.

At this stage we can only speculate about the forces that hold the cytochrome *bd*-I assemblages together. A network of protein–lipid and protein–protein interactions is likely to be involved. It is already known that cardiolipin is involved in the organization of respirasomes (Zhang *et al*., 2002; Pfeiffer *et al*., 2003) and that membrane lipids are heterogeneously distributed in the *E. coli* plasma membrane (Matsumoto *et al*., 2006). With specific regard to the *E. coli* cytochrome *bd*-I complex, its clustering may also involve YhcB, which has been identified as a putative third subunit of the complex by BN-PAGE (Stenberg *et al*., 2005) but has also been shown to have no role in the assembly or enzymatic activity of the complex (Mogi *et al*., 2006).

The existence of OXPHOS supercomplexes, discrete protein superstructures made up of various electron transport enzymes, in eukaryotic mitochondria and prokaryotes suggests that such structures may be characteristic of all respiratory membranes. While OXPHOS supercomplexes have not been identified in *E. coli*, this work emphasizes the theme that respiratory complexes are not freely diffusing 'lone-rangers' in bioenergetic membranes. In addition to this, by counting GFP molecules, we show that there are patches in the cell membrane of *E. coli* where large numbers of cytochrome *bd*-I complexes congregate. Even though we have visualized just one respiratory complex here, our observations in combination with the general apparent prevalence of OXPHOS supercomplexes lead us to suggest as a working hypothesis that respiration occurs in 'respira*zones*' – membrane patches dedicated to respiratory activity. If respirasomes do exist in *E. coli*, we propose that multiple respirasomes congregate in 'respira*zones*' (Lenn *et al*., 2008).

The respirazone hypothesis predicts the compartmentalization of membranes such that respiratory electron transport (and the associated redox sensing of the quinone pool) is segregated from other membrane functions by the concentration of respiratory enzymes within mobile domains. This is distinct from previous hypotheses about the organization of OXPHOS complexes in that it considers the organization of these complexes across the whole of the membrane surface rather than at the level of proteins and quinols.

We suggest that the physiological significance of respirasomes may be that membrane compartmentalization, particularly of a membrane that is multifunctional as in *E. coli*, improves the specificity of reactions of the quinol respiratory intermediates. In an uncompartmentalized membrane, reduced quinols could non-specifically reduce membrane components, which could be structurally damaging and would be wasteful of respiratory substrates. If the ATPase is also associated with respirazones, the efficiency of the proton circuit could also be enhanced by the close proximity of proton pumps and sinks as proton diffusion at the membrane surface leads to decay of the proton-motive force with increasing distance from the proton pump (Cherepanov *et al*., 2003). Further studies will be required to determine the full protein composition of respirazones and the extent to which quinone diffusion and the proton-motive force are localized to specific patches in the membrane. It also remains to be determined whether or not all the inhomogeneously distributed electron transport complexes participate equally in electron transport.

This work displays the potential of current fluorescence imaging technology on both biological and physical fronts. The high sensitivity of EMCCD technology and the improved contrast of both TIRF microscopy and FRAP-style pre-bleaching are combined here to resolve a unique combination of structural and dynamic detail in living cells, giving a new cellular perspective of a well-understood biochemical process.

On a more general level, our work shows that the plasma membrane of *E. coli* is heterogeneous on the 100 nm scale, with randomly distributed patches containing concentrations of a particular membrane protein. These patches are mobile on the subsecond timescale.

The bacterial plasma membrane appears to be a highly dynamic compartmentalized fluid.

Experimental procedures

Construction of E. coli *strain YTL01*

Strains and plasmids used are catalogued in Table S1, and the construction of the plasmid pYTL01 is illustrated in Fig. S1. PCR primers used are given in Table S2. *E. coli* BW25113 (wild type) and Keio:*cydB* (*cydB*-null) strains were obtained from NIG, Japan (Baba *et al*., 2006). The *E. coli* strain YTL01 was made in this study by a method based on that of Philippe *et al*. (2004). Here the *cydB–gfpuv4* fusion gene from the *cydB*–gfp ASKA plasmid (Kitagawa *et al*., 2005) and the 533 bp sequence downstream of the *cydAB* operon from BW25113 genomic DNA were PCR-amplified separately and then fused by overlap PCR (Shevchuk *et al*., 2004). The resultant construct contained an SphI restriction site in *cydB* and a PstI restriction site, which was added by PCR with overhanging primers to the 3′ end of the downstream 533 bp sequence. The construct and pDS132 were sequentially digested with PstI and SphI and the approximately 2.4 kb digestion product of the construct was ligated into the digested pDS132 to produce pYTL01, which was amplified and maintained in *pir*+ *E. coli* strain BW25141 (Datsenko and Wanner, 2000). Allelic exchange was effected between the chromosome of BW25113 and pYTL01 by chloramphenicol-sucrose counter-selection (Fig. 1). The wild-type BW25113 (*pir*–) was transformed with pYTL01 by electroporation. Chloramphenicol-resistant colonies, arising by integration of the pYTL01 into the chromosome of strain BW25113, were grown overnight in liquid culture without selection and plated onto sucrose plates to select for sucrose-resistant candidates where pYTL01 has been excised from the chromosome through a second recombination event. The desired sucrose-resistant chloramphenicol-sensitive phenotype of candidate recombinants was verified by replica-plating and candidate colonies were screened for the desired genotype by colony PCR with primers designed to anneal outside the sites of recombination. PCR products were sequenced to check that the GFP was correctly inserted and for point mutations.

Growth of cells

The YTL01, BW25113 and Keio:*cydB* strains were grown to the growth phase required for each experiment in aerobic batch culture in Luria–Bertani (LB) broth (Sambrook and Russell, 2001) at 37°C unless otherwise stated. The growth medium for Keio:*cydB* was supplemented with kanamycin (50 μg ml^{-1}).

Growth curves

Growth of *E. coli* strains in LB batch culture was monitored by inoculating 100 ml of LB (with 50 μg ml^{-1} kanamycin where appropriate) in a 250 ml conical flask with enough overnight culture to give cultures with identical initial OD_{600} values of 0.06. Cultures were shaken at 200 r.p.m. at 37°C and the OD_{600} was measured in a WPA Biowave II spectrophotometer at regular intervals.

Spectroscopy

Dithionite reduced-minus-air oxidized absorption spectra of whole cells in late exponential/early stationary phase were recorded by a Hitachi U3310 dual-beam spectrophotometer. Cells were grown to late exponential/early stationary phase in aerobic batch culture in LB medium and harvested by centrifugation. The pellets were re-suspended in 20% (w/v) Ficoll (Sigma F4375) solution and the samples placed into quartz cuvettes. The cell suspensions were oxidized by bubbling with air and a baseline spectrum was then recorded. A few grains of sodium dithionite (Sigma 157953) were then added to the cuvette and after a few minutes, when the spectrum was stable, the oxidized-minus-reduced spectrum was recorded. Cell concentrations were determined by OD_{600} values calibrated by a haemocytometer count.

Respiratory electron transport

O_2 uptake of cell cultures was measured at 37°C in a Clarke-type oxygen electrode (OxyLab 2, Hansatech, King's Lynn, UK). One millilitre of cell suspension from mid-exponential-phase aerobic LB batch culture was placed into the electrode chamber, aerated and sealed from the atmosphere. Hydroxylamine (Sigma 467804) was added to a final concentration of 30 mM in the reaction chamber when cells had reached a steady respiratory rate but had not yet used up all the oxygen in the medium.

SDS-PAGE and immunoblotting

Cells were grown overnight in liquid LB batch culture and fractionated as previously described (Randal and Hardy, 1986), to obtain cytoplasmic, periplasmic and membrane fractions. Proteins from each of the fractions were separated by SDS-PAGE (12.5% acrylamide) and semi-dry electroblotted onto a Hybond-P PVDF membrane (Amersham Biosciences). Washed blots were probed with anti-GFP antibodies (Abcam ab6556) and horseradish peroxidase anti-rabbit IgG conjugates and imaged using the Amersham ECL™ detection system (GE Healthcare) in a Typhoon™ 9200 Variable Mode Imager (GE Healthcare).

Microscopy

YTL01 cells were prepared for microscopy by adding 100 μl of overnight LB culture to 1 ml of minimal medium [M63-glucose (Atlas, 1993)] and incubating at room temperature without shaking in 1.5 ml microcentrifuge tubes for 3–4 h. Cells were then adhered to polylysine-coated coverslips and imaged at room temperature in a flow cell containing M63-glucose medium. Cells were imaged with a home-built inverted fluorescence microscope (Leake *et al*., 2006; Lo *et al*., 2006; 2007; Supporting Method S1). The microscope was used in both TIRF and epifluorescence modes with an

excitation wavelength of 473 nm. Fluorescence was imaged at 25 Hz with a pixel width of about 50 nm using a 128 × 128-pixel, cooled, back-thinned electron-multiplying charge-coupled device camera (iXon DV860-BI, Andor Technology, UK). Before switching to TIRF mode, the focal plane of the objective lens was set about 100 nm from the coverslip surface by focusing at the midpoint of fluorescent latex beads 200 nm in diameter. Images were sampled continuously, typically for about 50 s. Where appropriate, pre-bleaching was performed by application of an intense focused 473 nm laser spot of diameter ~1 μm to one pole of the cell, typically for about 0.5 s. This permitted single-particle tracking and quantitative stoichiometric measurements of fluorescent spots diffusing into the bleached region.

Data analysis

Images were subjected to automated tracking using custom-written code which measured the intensity, position and number of diffusing spots in single cells (Supporting Method S2), and CydB–GFP stoichiometry estimated by utilizing edge-detection algorithms (Leake *et al*., 2003; 2004) and Fourier analysis to measure the step-wise photobleaching of GFP (Leake *et al*., 2006; 2008; Supporting Method S3). Position data were used to measure diffusion for each spot and characterize anomalous behaviour (Supporting Method S4).

Acknowledgements

We thank Professor Peter Rich (University College London) for advice on spectroscopy and inhibitor assays; Dr Anja Nenninger (Queen Mary, University of London) for instruction on cell fractionation and immunoblotting; Professor Judith Armitage, Dr George Wadhams and Mr Nicolas Delalez (University of Oxford) for advice on mutagenesis and facilitating the collaboration between C.W.M., T.L. and M.C.L. We thank Thorsten Friedrich (University of Freiburg) for helpful discussion and communicating preliminary results. M.C.L. is supported by a Royal Society University Research Fellowship. T.L. is supported by a College Research Studentship (Queen Mary, University of London). Research was supported by grants to T.L. from the University of London Central Research Fund and to C.W.M. from the Biotechnology and Biological Sciences Research Council.

References

Atlas, R.M. (1993) *Handbook of Microbiological Media.* Boca Raton, FL: CRC Press.

Baba, T., Ara, T., Hasegawa, M., Takai, Y., Okumura, Y., Baba, M., *et al*. (2006) Construction of *Escherichia coli* K-12 in-frame single-gene knockout mutants: the Keio collection. *Mol Syst Biol* **2:** 2006.0008.

Boekema, E.J., and Braun, H.P. (2007) Supramolecular structure of the mitochondrial oxidative phosphorylation system. *J Biol Chem* **282:** 1–4.

Cherepanov, D.A., Feniouk, B.A., Junge, W., and Mulkidjanian, A.Y. (2003) Low dielectric permittivity of water at the membrane interface: effect on the energy coupling mechanism in biological membranes. *Biophys J* **85:** 1307–1316.

Cotter, P.A., Chepuri, V., Gennis, R.B., and Gunsalus, R.P. (1990) Cytochrome *o* (*cyoABCDE*) and *d* (*cydAB)* oxidase gene expression in *Escherichia coli* is regulated by oxygen, pH, and *fnr* gene product. *J Bacteriol* **172:** 6333–6338.

Dassa, J., Fsihi, H., Marck, C., Dion, M., Kieffer-Bontemps, M., and Boquet, P.L. (1991) New oxygen-regulated operon in *Escherichia coli* comprises the genes for a putative third cytochrome oxidase and for pH 2.5 acid phosphatase (*appA*). *Mol Genet Genomics* **229:** 341–352.

Datsenko, K.A., and Wanner, B.L. (2000) One-step inactivation of chromosomal genes in *Escherichia coli* K-12 using PCR products. *Proc Natl Acad Sci USA* **97:** 6640–6645.

Dudkina, N.V., Heinemeyer, J., Sunderhaus, S., Boekema, E.J., and Braun, H.-P. (2006) Respiratory chain supercomplexes in plant mitochondrial membrane. *Trends Plant Sci* **11:** 232–240.

Engelman, D.M. (2005) Membranes are more mosaic than fluid. *Nature* **438:** 578–580.

Green, R., and Gennis, R.B. (1983) Isolation and characterization of an *Escherichia coli* mutant lacking cytochrome *d* terminal oxidase. *J Bacteriol* **154:** 1269–1275.

Gross, D.J., and Webb, W.W. (1988) Cell surface clustering and mobility of the liganded LDL receptor measured by digital video fluorescence microscopy. In *Spectroscopic Membrane Probes II.* Loew, L.M. (ed.). Boca Raton, FL: CRC Press, pp. 19–45.

Ito, Y., Suzuki, M., and Husimi, Y. (1999) A novel mutant of green fluorescent protein with enhanced sensitivity for microanalysis at 488 nm excitation. *Biochem Biophys Res Comm* **264:** 556–560.

Iuchi, S., Chepuri, V., Gennis, R.B., and Lin, E.C.C. (1990) Requirement for terminal cytochromes in generation of the aerobic signal for the *arc* regulatory system in *Escherichia coli:* study utilizing deletions and *lac* fusion of *cyo* and *cyd*. *J Bacteriol* **172:** 6020–6025.

Iverson, T.M., Luna-Chavez, C., Cecchini, G., and Rees, D.C. (1999) Structure of the *Escherichia coli* fumarate reductase respiratory complex. *Science* **284:** 1961–1966.

Johnson, A.S., van Horck, S., and Lewis, P.J. (2004) Dynamic localisation of membrane proteins in *Bacillus subtilis*. *Microbiology* **150:** 2815–2824.

Kita, K., Konishi, K., and Araku, Y. (1984) Terminal oxidases of *Escherichia coli* aerobic respiratory chain. *J Biol Chem* **259:** 3368–3381.

Kitagawa, M., Ara, T., Arifuzzaman, M., Ioka-Nakamichi, T., Inamoto, E., Toyonaga, H., and Mori, H. (2005) Complete set of ORF clones of *Escherichia coli* ASKA library (*A* Complete *S*et of *K*-12 ORF *A*rchive): unique resources of biological research. *DNA Res* **12:** 291–299.

Kusumi, A., Sako, Y., and Yamamoto, M. (1993) Confined lateral diffusion of membrane receptors as studied by single particle tracking (nanovid microscopy). Effects of calcium-induced differentiation in cultured epithelial cells. *Biophys J* **65:** 2021–2040.

Kusumi, A., Nakada, C., Ritchie, K., Murase, K., Suzuki, K., Murakoshi, H., *et al*. (2005) Paradigm shift of the plasma membrane concept from the two-dimensional continuum fluid to the partitioned fluid: high-speed single molecule tracking of membrane molecules. *Annu Rev Biophys Biomolec Struct* **34:** 351–378.

Leake, M.C., Wilson, D., Bullard, B., and Simmons, R.M.

(2003) The elasticity of single kettin molecules using a two-bead laser-tweezers assay. *FEBS Lett* **535:** 55–60.

Leake, M.C., Wilson, D., Gautel, M., and Simmons, R.M. (2004) The elasticity of single titin molecules using a two-bead optical tweezers assay. *Biophys J* **87:** 1112–1135.

Leake, M.C., Chandler, J.H., Wadhams, G.H., Fan, B., Berry, R.M., and Armitage, J.A. (2006) Stoichiometry and turnover in single, functioning membrane protein complexes. *Nature* **443:** 355–358.

Leake, M.C., Greene, N.P., Godun, R.M., Granjon, T., Buchanan, G., Chen, S., *et al.* (2008) Variable stoichiometry of the TatA component of the twin-arginine protein transport system observed by *in vivo* single-molecule imaging. *Proc Natl Acad Sci USA* **105:** 15376–15381.

Lenaz, G., and Genova, M.L. (2007) Kinetics of integrated electron transfer in the mitochondrial respiratory chain: random collisions vs. solid state electron channeling. *Am J Physiol Cell Physiol* **292:** C1221–C1239.

Lenn, T., Leake, M.C., and Mullineaux, C.W. (2008) Are *Escherichia coli* OXPHOS complexes concentrated in specialized zones within the plasma membrane? *Biochem Soc Trans* **36:** 1032–1036.

Lo, C.-J., Leake, M.C., and Berry, R.M. (2006) Fluorescence measurement of intracellular sodium concentration in single *Escherichia coli* cells. *Biophys J* **90:** 357–365.

Lo, C.-J., Leake, M.C., Pilizota, T., and Berry, R.M. (2007) Nonequivalence of membrane voltage and ion-gradient as driving forces for the bacterial flagellar motor at low load. *Biophys J* **93:** 294–302.

Marguet, D., Lenne, P.-F., Rigneault, H., and He, H.-T. (2006) Dynamics in the plasma membrane: how to combine fluidity and order. *EMBO* **25:** 3446–3457.

Matsumoto, K., Kusaka, J., Nishibori, A., and Hara, H. (2006) Lipid domains in bacterial membranes. *Mol Microbiol* **61:** 1110–1117.

Meunier, B., Madgwick, S.A., Reil, E., Oettmeier, W., and Rich, P. (1995) New inhibitors of the quinol oxidation sites of bacterial cytochromes *bo* and *bd*. *Biochemistry* **34:** 1076–1083.

Miller, M.J., and Gennis, R.B. (1983) The purification and characterisation of the cytochrome *d* terminal oxidase complex of the *Escherichia coli* aerobic respiratory chain. *J Biol Chem* **258:** 9159–9165.

Mogi, T., Mizuochi-Asai, E., Endou, S., Akimoto, S., and Nakamura, H. (2006) Role of putative third subunit YhcB on the assembly and function of cytochrome *bd*-type ubiquinol oxidase from *Escherichia coli*. *Biochim Biophys Acta-Bioenerg* **1757:** 860–864.

Pfeiffer, K., Gohil, V., Stuart, R.A., Hunte, C., Brandt, U., Greenberg, M.L., and Schägger, H. (2003) Cardiolipin stabilizes respiratory chain supercomplexes. *J Biol Chem* **278:** 52873–52880.

Philippe, N., Alcaraz, J.-P., Coursange, E., Geiselmann, J., and Schneider, D. (2004) Improvement of pCVD442, a suicide plasmid for gene allele exchange in bacteria. *Plasmid* **51:** 246–255.

Randall, L.L., and Hardy, S.J.S. (1986) Correlation of competence for export with lack of tertiary structure of the mature species: a study *in vivo* of maltose-binding protein in *E. coli*. *Cell* **46:** 921–928.

Rich, P.R. (2003) The molecular machinery of Keilin's respiratory chain. *Biochem Soc Trans* **31:** 1095–1105.

Sambrook, J., and Russell, D.W. (2001) *Molecular Cloning: A Laboratory Manual.* Plainview, NY: Cold Spring Harbor Laboratory Press.

Schäfer, E., Seelert, H., Reifschneider, N.H., Krause, F., Dencher, N.A., and Vonck, J. (2006) Architecture of active mammalian respiratory chain supercomplexes. *J Biol Chem* **281:** 15370–15375.

Schägger, H. (2002) Respiratory chain supercomplexes of mitochondria and bacteria. *Biochim Biophys Acta-Bioenerg* **1555:** 154–159.

Shevchuk, N.A., Bryksin, A.V., Nusinovich, Y.A., Cabello, F.C., Sutherland, M., and Ladisch, S. (2004) Construction of long DNA molecules using long PCR-based fusion of several fragments simultaneously. *Nucleic Acids Res* **32:** e19.

Singer, S.J., and Nicholson, G.L. (1972) The fluid mosaic model of the structure of cell membranes. *Science* **175:** 720–731.

Stenberg, F., Chovanec, P., Maslen, S.L., Robinson, C.V., Ilag, L.L., von Heijne, G., and Daley, D.O. (2005) Protein complexes in the *Escherichia coli* cell envelope. *J Biol Chem* **280:** 34409–34419.

Sturr, M.G., Krulwich, T.A., and Hicks, D.B. (1996) Purification of a cytochrome *bd* terminal oxidase encoded by the *Escherichia coli app* locus from a Δ*cyo* Δ*cyd* strain complemented by genes from *Bacillus firmus* OF4. *J Bacteriol* **178:** 1742–1749.

Tsubaki, M., Hiroshi, H., Mogi, T., and Anraku, Y. (1995) Cyanide-binding site of *bd*-type ubiquinol oxidase from *Escherichia coli*. *J Biol Chem* **270:** 28565–28569.

Unden, G., and Bongaerts, J. (1997) Alternative respiratory pathways of *Escherichia coli*: energetics and transcriptional regulation in response to electron acceptors. *Biochim Biophys Acta-Bioenerg* **1320:** 217–234.

Zhang, J., Barquera, B., and Gennis, R.B. (2004) Gene fusions with β-lactamase show that subunit I of the cytochrome *bd* quinol oxidase from *E. coli* has nine transmembrane helices with the O_2 reactive site near the periplasmic surface. *FEBS Lett* **561:** 58–62.

Zhang, M., Mileykovskaya, E., and Dowhan, W. (2002) Gluing the respiratory chain together. *J Biol Chem* **277:** 43553–43556.

Supporting information

Additional supporting information may be found in the online version of this article.

Please note: Wiley-Blackwell are not responsible for the content or functionality of any supporting materials supplied by the authors. Any queries (other than missing material) should be directed to the corresponding author for the article.

